Celal Bayar University Journal of Science

Selectively Nanocube Formation of Tungsten Oxide (WO_3)

Tugay Üstün[1]*, Volkan Eskizeybek[2], Ahmet Avcı[3]

[1]Başkent University, Kahramankazan Vocational School, Ankara, TURKEY
[2]Çanakkale Onsekiz Mart University, Engineering Faculty, Materials Science and Engineering Department, Çanakkale, TURKEY
[3]Necmettin Erbakan University, Engineering and Architecture Faculty, Biomedical Engineering Department, Konya, TURKEY
*tugayustun@baskent.edu.tr
*Orcid: 0000-0001-5365-3054

Received: 20 January 2020
Accepted: 15 June 2020
DOI: 10.18466/ cbayarfbe.677407

Abstract

Metal oxide nanoparticles with tunable size and shape are of significant interest since these features allow tailoring their performance, functionality, and efficiency. Doping of metal oxide nanoparticles with metal cations proved to be an effective strategy for tailoring their electrical, optical, and microstructural properties. In this study, tungsten oxide (WO_3) nanoparticles doped with selenium (Se) and lanthanum (La) catalysts were produced with a preferential nanocube morphology by arc discharge method. Se and La catalysts were introduced into the tungsten (W) electrode acting as an anode, and the arc-discharge was generated between two W electrodes in a deionized water medium. Structural and morphological features of the as-synthesized nanostructures were investigated by performing scanning electron microscopy (SEM) and transmission electron microscopy (TEM) analyses. Morphological analyses revealed that the resultant nanoparticles exhibited nanocube morphology with size ranges of 10 to 50 nm. X-ray diffraction (XRD) results proved the existence of highly crystalline monoclinic WO_3 as an abundant structure. We confidently believe that the arc-discharge method can be utilized to produce various types of nanostructures with tunable size and shape by tailoring process parameters, including the type of dopant.

Keywords: Arc discharge, catalyst, nanocube, WO_3.

1. Introduction

Metal oxide nanostructures constitute a significant area of interest within the field of nanotechnology due to their crucial role in the development of smart devices and functional materials. Recently, numerous research endeavors have focused on the development of metal oxide nanoparticles and their engineering applications such as solar cells and gas sensors. Tungsten oxide (WO_x) plays a pivotal role in the development of nanotechnology-based applications due to its different levels of oxidation [1]. This makes it a valuable metal oxide, allowing a wide range of applications such as bio-molecule sensors [2], solar cells [3], waste-water treatment [4], electrochromic [3] and photochromic applications [3].

Among other types of WO_x, tungsten (VI) oxide (WO_3) is a non-toxic n-type semiconductor (2.6-3.7 eV), which is utilized as a functional layer in smart devices and functional materials [5]. WO_3 nanoparticles are obtained in various morphologies including nanowire [6], nanorod [7], nanoflake [8], and nanotube [9]. The variety of these morphologies can be achieved by introducing various metal catalysts in the synthesis medium such as Cu [10], Sn [11], Mn [12], and La [13]. It is now well established that chemical and physical performance of metal oxide nanostructures such as electrical and thermal conductivities are primarily governed by their size and morphology [13]. Cubic shaped nanoparticles can be specifically utilized in biomedical applications [14] due to their higher surface area allowing for the surface modification with bio-functional groups [15].

Celal Bayar University Journal of Science
Volume 16, Issue 2, 2020, p 149-153
Doi: 10.18466/cbayarfbe.677407

Doping metal oxide nanoparticles during their synthesis with metal cations could likely have an enormous impact on desired physical and chemical features. Se and La, which are the rare earth elements, are utilized as dopants to tailor desired properties of various nanostructures [16]. While Se doping has been specifically used to improve electrocatalytic performance of carbon-based nanostructures [17], La is mainly utilized as a phase stabilizer or to increase the photocatalytic efficiency [18].

There are various production methods introduced in the literature for WO_3 nanoparticles such as hydrothermal [19], sol-gel [20], thermal decomposition [3], and arc discharge [21]. Arc discharge submerged in a liquid medium has become an effective process to synthesize various types of nanoparticles due to its significant advantages such as large-scale synthesis, simple and cost-effectiveness [22]. This facile method can be effectuated with a dc power supply and an open vessel full of a liquid medium without a need of vacuum media, furnace, and reacted gases such as argon, nitrogen, helium or hydrogen compared with any other well-known methods [22]. Production of nanoparticles such as fullerene [23], carbon nanotube (CNT) [24], carbon nano-onion [25], ZnO [26] and $Cd(OH)_2$ [22] was realized by arc discharge method. Moreover, various liquid environments including deionized water, liquid nitrogen, and mineral water were adopted.

So far, however, there has been little discussion about the morphology control of WO_3 nanostructures during synthesis. In this study, we discuss the production and characterization of WO_3 nanoparticles with a nanocube morphology using selenium and lanthanum as metal catalysts. We have prepared WO_3 nanostructures by the arc discharge method in deionized water which aids to oxidize the tungsten particles and form tungsten oxide. Structural and morphological properties of WO_3 nanostructures were examined.

2. Materials and Methods

All the chemicals were of analytical grade and used as received without further purification. W rods with a 12 mm diameter (99.99%) were used as anode and cathode electrodes and purchased from Alfa Aesar. Cathode electrode weighed 98 grams. Se and La powders with high purity (-200 mesh, 99.999%) were also supplied by Alfa Aesar. Deionized water was used throughout.

WO_3 nanostructures were synthesized using an arc-discharge apparatus as shown in Figure 1. Three identical holes with a diameter of 3 mm and depth of 5 mm were drilled on the anode electrode and 0.2 g of Se and La catalyst mixture (50:50 wt%) was filled into the holes. After submerging the apparatus into the deionized water, the anode electrode was adjusted with a control screw up to initiate the arc current. During this contact, the arc current provided by a direct current (DC) power supply was applied as 50 A. This current value is obtained from several experimental studies and it is the ideal current value for producing large amounts and optimal dimensions of metal oxide nanoparticles [22]. In the case of electrodes in contact with each other, the anode electrode consumes and the temperature during arc-discharge also rises up to 5000°K [23]. The arc discharge was continued for almost 4 min, and the discharge voltage was measured by a multimeter to achieve a stable arc. Following, the produced particles were allowed to rest in the reaction vessel at room temperature for 24 h. After, the collected particles are washed with deionized water and dried under vacuum at 40°C for 24 h.

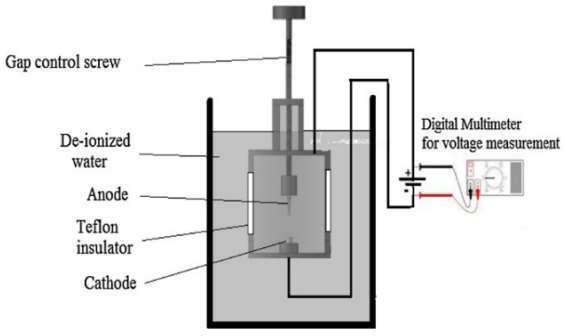

Figure 1. Schematic view of the arc-discharge apparatus [22]

The crystal structure, particle sizes and morphologies of the produced nanoparticles were determined by means of X-ray diffraction (XRD), Fourier transform infrared (FTIR), scanning electron microscopy (SEM) and transmission electron microscopy (TEM). XRD analysis was performed by Shimadzu XRD-6000 X-ray diffractometer using Cu Ka (k = 0.15418 nm) radiation at 40 kV and 30 mA ranging from 2 to 80° at a scanning rate of 2°/ min. FTIR spectra were recorded by a Perkin-Elmer 1725 instrument. Morphological properties of nanoparticles were analyzed by using JEOL / JSM-6335F-EDS SEM, JEOL 2100 HRTEM (at 300 kV).

3. Results and Discussion

The XRD pattern of as-synthesized particles produced by the arc discharge method are given in Figure 2a. The XRD pattern shows the coexistence of three phases including monoclinic WO_3 (m-WO_3), α-W and β-W. The lattice structure parameters of m-WO3 are shown as a=0.7297 nm, b=0.7539 nm and c=0.7688 nm (JCPDS: 43-1035). The disordered characteristics of m-WO_3 phase indicates almost amorphous phase. It can be seen from the XRD pattern that WO_3 nanoparticles exhibit preferential orientation in the (002), (020) and (200) directions. Wang et al. reported the formation of cubic

m-WO_3 nanoparticles exhibiting similar preferential orientation [27]. The calculated Scherrer crystallites size of m-WO3 phase (i.e. crystalline coherent domains) is about 16.5 nm. The sharp and strong peaks on the XRD patterns allow the determination of the purity and dimensions of the produced nanostructures [28]. In addition, the dominant crystalline phases as the α-W and β-W are also detectable on the XRD pattern. The α-W presents a lattice parameter a = 0.3166 nm, close to the standard value of a = 0.31648 nm (JCPDS 04-0806), and Scherrer crystallites size of 44.5 nm. The lattice parameter of the β-W phase is a= 0.504 nm, comparable to the standard value of 0.505 nm (JCPDS 47-1319); the Scherrer crystallites size is 47 nm, in the same range as the main α-W phase. We confidently believe that α-W and β-W phases are formed due to insufficient oxygen in the aqueous medium during forming of the m-WO_3 nanoparticles. Accordingly, similar results can be seen in the EDS spectrum (Figure 2b). As a result of the EDS analysis, there were no different atoms in the structure and the desired purity was achieved.

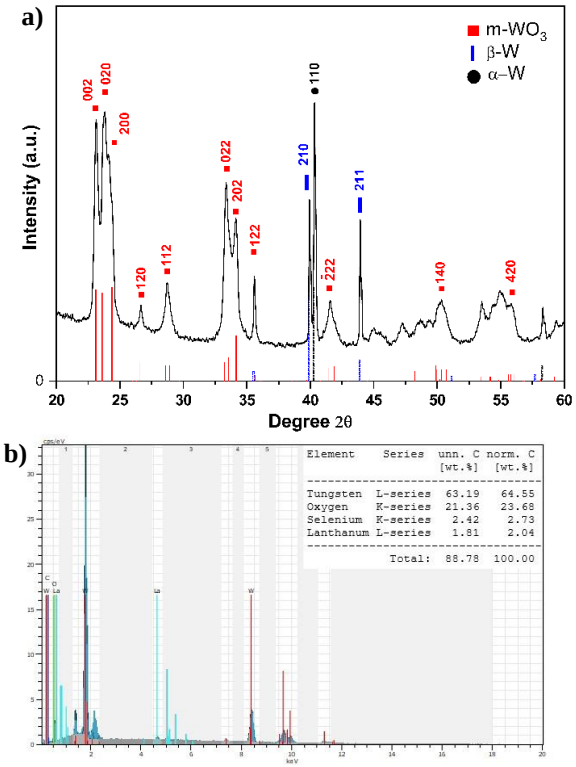

Figure 2. a) XRD patterns of Se-La containing monoclinic WO_3 nanocubes b) EDS spectrum showing tungsten, oxygen, selenium and lanthanum contained in WO_3 nanocubes.

Figure 3 shows SEM images of WO_3 nanoparticles settled at the bottom of the reaction vessel as produced by arc discharge in deionized water with an arc current of 50 A. It is seen that WO_3 nanoparticles are agglomerated with an average size of 10-50 nm.

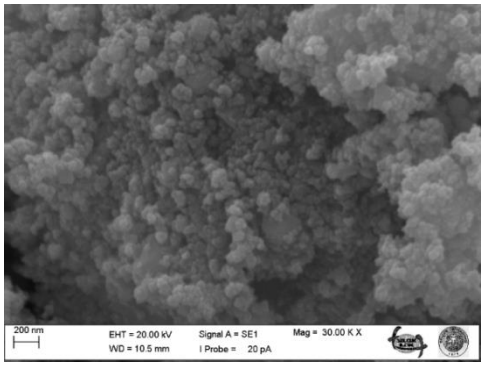

Figure 3. SEM images of WO_3 nanocubes

TEM and high resolution TEM images of the WO_3 nanoparticles are shown in Figure 4. In Figure 4a, it is seen that the WO_3 nanoparticles are preferably exhibit cubic morphology. It can also be measured that the average dimensions of these cube structures are between 10 and 50 nm as confirmed by SEM analysis. The lattice spacing from the high resolution TEM image is measured at approximately 0.37 nm (Figure 4b inset). This value indicates that the monoclinic structure of the WO_3 with good crystallinity [28].

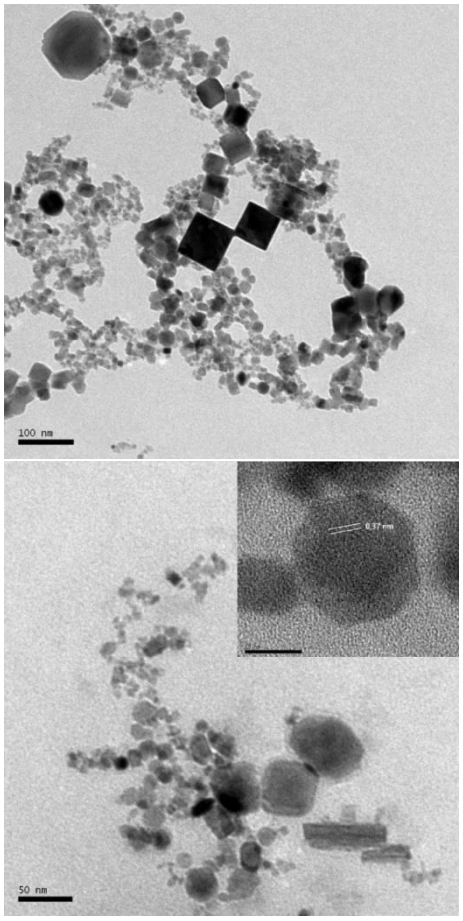

Figure 4. TEM images of WO_3 nanocubes. The scale in the pictures is 100 nm, 50 nm and 10 nm respectively.

The produced WO_3 nanoparticles were further analyzed by Fourier transform infrared (FTIR) spectroscopy and shown in Figure 5. In the WO_3 crystal, the IR band of the O-W-O bond is generally between 600 and 900 cm^{-1} [29]. In addition, the other peak in the IR spectrum (1650 cm^{-1}) shows H-O stretching [29].

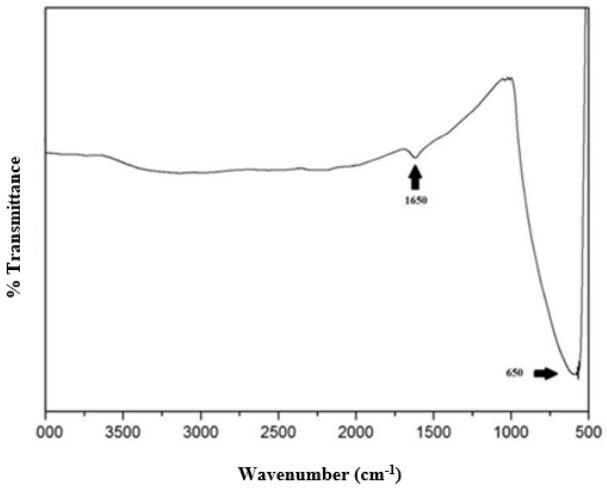

Figure 5. FTIR spectrum of the WO_3 nanocubes

4. Conclusion

In this study, Se and La catalysts were added and WO_3 nanocubes were produced by the arc discharge method in the deionized water environment. With this method, a large amount of homogeneous distribution allows the production of nanocubes. XRD, SEM, EDS, TEM and FTIR analyzed the crystalline and morphological structure of the WO_3 nanocubes with catalyst addition. XRD analysis shows that Se and La are involved in this production and WO_3 nanocubes have a monoclinic crystal structure. While these nanocubes are seen with TEM images, where the dimensions are between 10-50 nm, the high surface-to-volume ratio provides an important advantage in applications.

Acknowledgements

The authors are grateful for Technical support from the Selçuk University Advanced Technology Research and Application Center is much appreciated. Mert Akgün from the Canakkale Onsekiz Mart University Science and Technology Application and Research Center (COBILTUM) is also acknowledged for his assistance and suggestions.

Ethics

There are no ethical issues after the publication of this manuscript

References

[1]. Supothina, S, Seeharaj, P, Yoriya, S, Sriyudthsak, M. 2007. Synthesis of tungsten oxide nanoparticles by acid precipitation method. *Ceramics International*; 33(6): 931-936.

[2]. Anithaa, AC, Lavanya, N, Asokan, K, Sekar, C. 2015. WO3 nanoparticles based direct electrochemical dopamine sensor in the presence of ascorbic acid. *Electrochimica Acta*; 167: 294-302.

[3]. Yan, H, Zhang, X, Zhou, S, Xie, X, Luo, Y, Yu, Y. 2011. Synthesis of WO 3 nanoparticles for photocatalytic O 2 evolution by thermal decomposition of ammonium tungstate loading on gC 3 N 4. *Journal of Alloys and Compounds*; 509(24): L232-L235.

[4]. Bamwenda, GR, Arakawa, H. 2001. The visible light induced photocatalytic activity of tungsten trioxide powders. *Applied Catalysis A: General*; 210(1): 181-191.

[5]. Villa, K, Murcia-López, S, Morante, JR, Andreu, T. 2016. An insight on the role of La in mesoporous WO 3 for the photocatalytic conversion of methane into methanol. *Applied Catalysis B: Environmental*; 187: 30-36.

[6]. Gu, Z, Li, H, Zhai, T, Yang, W, Xia, Y, Ma, Y, Yao, J. 2007. Large-scale synthesis of single-crystal hexagonal tungsten trioxide nanowires and electrochemical lithium intercalation into the nanocrystals. *Journal of Solid State Chemistry*; 180(1): 98-105.

[7]. Wang, J, Khoo, E, Lee, PS, Ma, J. 2008. Synthesis, assembly, and electrochromic properties of uniform crystalline WO3 nanorods. *The Journal of Physical Chemistry C*; 112(37): 14306-14312.

[8]. Supothina, S, Seeharaj, P, Yoriya, S, Sriyudthsak, M. 2007. Synthesis of tungsten oxide nanoparticles by acid precipitation method. *Ceramics International*; 33(6): 931-936.

[9]. Li, Y, Bando, Y, Golberg, D. 2003. Quasi-Aligned Single-Crystalline W18O49 Nanotubes and Nanowires. *Advanced Materials*; 15(15): 1294-1296.

[10]. Bai, X, Ji, H, Gao, P, Zhang, Y, Sun, X. 2014. Morphology, phase structure and acetone sensitive properties of copper-doped tungsten oxide sensors. *Sensors and Actuators B: Chemical*; 193: 100-106.

[11]. Upadhyay, SB, Mishra, RK, Sahay, PP. 2014. Structural and alcohol response characteristics of Sn-doped WO 3 nanosheets. *Sensors and Actuators B: Chemical*; 193: 19-27.

[12]. Abhudhahir, MHS, Kandasamy, J. 2015. Photocatalytic effect of manganese doped WO3 and the effect of dopants on degradation of methylene blue. *Journal of Materials Science: Materials in Electronics*; 26(11): 8307-8314.

[13]. Li, J, Cheng, J, Wei, B, Zhang, M, Luo, L, Wu, Y. 2017. Microstructure and properties of La 2 O 3 doped W composites prepared by a wet chemical process. *International Journal of Refractory Metals and Hard Materials*; 66: 226-233.

[14]. Abbas, M, Takahashi, M, Kim, C. 2013. Facile sonochemical synthesis of high-moment magnetite (Fe3O4) nanocube. *Journal of nanoparticle research*; 15(1): 1354.

[15]. O'Kelly, C, Jung, SJ, Bell, AP, Boland, JJ. 2012. Single crystal iron nanocube synthesis via the surface energy driven growth method. *Nanotechnology*; 23(43): 435604.

[16]. Sibu, CP, Kumar, SR, Mukundan, P, Warrier, KGK. 2002. Structural modifications and associated properties of lanthanum

oxide doped sol−gel nanosized titanium oxide. *Chemistry of Materials*; *14*(7): 2876-2881.

[17]. Jin, Z, Nie, H, Yang, Z, Zhang, J, Liu, Z, Xu, X, Huang, S. 2012. Metal-free selenium doped carbon nanotube/graphene networks as a synergistically improved cathode catalyst for oxygen reduction reaction. *Nanoscale*; *4*(20): 6455-6460.

[18]. Derk, AR, Li, B, Sharma, S, Moore, GM, McFarland, EW, Metiu, H. 2013. Methane oxidation by lanthanum oxide doped with Cu, Zn, Mg, Fe, Nb, Ti, Zr, or Ta: the connection between the activation energy and the energy of oxygen-vacancy formation. *Catalysis letters*; *143*(5): 406-410.

[19]. Hong, SJ, Jun, H, Borse, PH, Lee, JS. 2009. Size effects of WO 3 nanocrystals for photooxidation of water in particulate suspension and photoelectrochemical film systems. *International Journal of Hydrogen Energy*; 34(8): 3234-3242.

[20]. Gondal, MA, Dastageer, MA, Khalil, A. 2009. Synthesis of nano-WO 3 and its catalytic activity for enhanced antimicrobial process for water purification using laser induced photo-catalysis. *Catalysis Communications*; 11(3): 214-219.

[21]. Ospina, R, Castillo, HA, Benavides, V, Restrepo, E, Arango, YC, Arias, DF, Devia, A. 2006. Influence of the annealing temperature on a crystal phase of W/WC bilayers grown by pulsed arc discharge. *Vacuum*; 81(3): 373-377.

[22]. Eskizeybek, V, Avcı, A, Chhowalla, M. 2011. Structural and optical properties of CdO nanowires synthesized from Cd (OH) 2 precursors by calcination. *Crystal Research and Technology*; 46(10): 1093-1100.

[23]. Qiu, G, Dharmarathna, S, Zhang, Y, Opembe, N, Huang, H, Suib, SL. 2011. Facile microwave-assisted hydrothermal synthesis of CuO nanomaterials and their catalytic and electrochemical properties. *The Journal of Physical Chemistry C;* 116(1): 468-477.

[24]. Krätschmer, W, Lamb, LD, Fostiropoulos, K, Huffman, DR. 1990. Solid C60: a new form of carbon. *Nature;* 347(6291): 354-358.

[25]. Ashkarran, AA, Mahdavi, SM, Ahadian, MM. 2010. Photocatalytic activity of ZnO nanoparticles prepared via submerged arc discharge method. *Applied Physics A;* 100(4): 1097-1102.

[26]. Fang, F, Futter, J, Markwitz, A, Kennedy, J. 2009. UV and humidity sensing properties of ZnO nanorods prepared by the arc discharge method. *Nanotechnology;* 20(24): 245502.

[27]. Wang, L, Hu, H, Xu, J, Zhu, S, Ding, A, Deng, C. 2019. WO3 nanocubes: Hydrothermal synthesis, growth mechanism, and photocatalytic performance. *Journal of Materials Research*; *34*(17): 2955-2963.

[28]. Guery, C, Choquet, C, Dujeancourt, F, Tarascon, JM, Lassegues, JC. 1997. Infrared and X-ray studies of hydrogen intercalation in different tungsten trioxides and tungsten trioxide hydrates. *Journal of Solid State Electrochemistry*; 1(3): 199-207.

[29]. Mao, L, Liu, C. 2008. A new route for synthesizing VO 2 (B) nanoribbons and 1D vanadium-based nanostructures. *Materials Research Bulletin*; 43(6): 1384-1392.